Applied Catalysis B: Environmental 203 (2017) 400–407

Contents lists available at ScienceDirect

Applied Catalysis B: Environmental

journal homepage: www.elsevier.com/locate/apcatb

# Innovative $ZrO_2$-supported CuPd catalysts for the selective production of hydrogen from methanol steam reforming

C.S.R. Azenha[a], C. Mateos-Pedrero[a,*], S. Queirós[a], P. Concepción[b], A. Mendes[a,*]

[a] LEPABE – Departamento de Engenharia Química, Faculdade de Engenharia da Universidade do Porto, Rua Dr. Roberto Frias, 4200-465 Porto, Portugal
[b] Instituto de Tecnología Química, UPV-CSIC, Avda. de los Naranjos s/n, 46022 Valencia, Spain

ARTICLE INFO

*Article history:*
Received 18 July 2016
Received in revised form 10 October 2016
Accepted 15 October 2016
Available online 17 October 2016

*Keywords:*
CO-selectivity
Zirconia
Methanol steam reforming
Palladium
Copper

ABSTRACT

Low temperature methanol steam reforming (MSR) is an attractive source of nearly CO-free $H_2$ for fuel cells application. However, there is still a lack of efficient catalysts able to operate at low temperatures ($\leq$220 °C), where MSR is equilibrium-limited. Pd-based catalysts are regarded as an alternative to conventional Cu-based catalysts for MSR, but their low MSR selectivity limit their application. This work studies the effect of Cu as MSR promoter of Pd/$ZrO_2$ catalysts, with special emphasis on the improvement of MSR selectivity. The influence of $ZrO_2$ structure support, monoclinic and cubic, on the MSR behavior is also studied. CuPd/$ZrO_2$-m catalysts with enhanced activity and MSR selectivity are developed. This superior performance was attributed to a strong interaction between Pd and Cu and an enhanced dispersion of the metal phase when $ZrO_2$ with monoclinic structure was used as support.



## 1. Introduction

Highly fluctuating costs of petroleum derived fuels and environmental and security concerns have driven research into new and clean sources of energy. $H_2$ has long been regarded as a promising energy vector alternative to fossil fuels [1,2] and fuel cells are expected to have a key role as high efficiency energy converting devices [3]. Despite being the best fuel for polymer electrolyte membrane fuel cells (PEMFC), handling and storage of an explosive gas such as hydrogen requires special conditions and special materials to minimize diffusion and leakages. For this reason fuel processors that can convert liquid fuel into $H_2$ have attracted great interest [4].

Among the different hydrogen feedstocks available, methanol has been extensively studied in recent years due to its several advantages: it is liquid at room temperature, has high H/C ratio and low propensity for soot formation [2]. Therefore, the refueling system required is compatible with present gasoline distribution infrastructures [4]. Methanol can be converted into $H_2$ by different chemical reactions, among them Methanol Steam Reforming (MSR) Reaction (1) provides the highest amount of $H_2$.

$$CH_3OH + H_2O \leftrightarrow 3H_2 + CO_2 \quad \Delta H^\circ = 49.7\,kJ\,mol^{-1} \qquad (1)$$

MSR is accompanied with side reactions, resulting in the production of CO as by-product [2]. In order to avoid poisoning of the Pt anode of the fuel cell, CO formation must be strongly minimized. Since CO is mainly formed by the highly endothermic methanol decomposition (MD) reaction, the low temperature MSR (LT-MSR) is an attractive source of nearly CO-free $H_2$. Nevertheless, the design of the catalyst is still crucial in order to achieve high methanol conversion with low CO formation [5].

Cu-based catalysts are the most commonly used for MSR and several improvement approaches are reported in literature, from the addition of promoters to the employment of different preparation methods [2]. Even so, pyrophoricity, easy deactivation and poor thermal stability remain characteristic of this type of catalysts [5,6]. The search for a more suitable catalyst for MSR has led to the discovery of a different type of Pd catalysts that exhibited extremely low CO production [7]. The unusual behavior of these Pd-based catalysts was attributed to the formation of a PdMe alloy (Me = Zn, Ga, In) upon proper reductive pre-treatment, which modifies the catalytic function of Pd [8].

The present work studies the effect of Cu as MSR promoter of Pd/$ZrO_2$ catalysts, with special emphasis on the improvement of MSR selectivity. $ZrO_2$ was used as carrier since this support material has already demonstrated interesting catalytic properties in

* Corresponding authors.
*E-mail addresses:* cmpedrero@fe.up.pt (C. Mateos-Pedrero), mendes@fe.up.pt (A. Mendes).

http://dx.doi.org/10.1016/j.apcatb.2016.10.041
0926-3373/

MSR [9,10]. $ZrO_2$ has three polymorphs (monoclinic, tetragonal and cubic) that significantly influence the activity of catalysts, as already reported in literature [11]. Thus, the influence of the $ZrO_2$ crystalline structure (monoclinic and cubic) on the performance of Pd-based catalysts for MSR was also evaluated. To the best of our knowledge, this is the first study reporting on $CuPd/ZrO_2$ catalyst for MSR.

## 2. Experimental

### 2.1. Synthesis of $ZrO_2$ supports

All reagents were used without any pre-treatment. The $ZrO_2$ supports were obtained by precipitation of $ZrO(NO_3)_2$ (Wako-Chemicals) with $NH_4OH$, as an adaption of the methodology proposed by Bokhimi et al. [12]. The appropriated yttrium nitrate amount was added in order to stabilize the different crystalline phases of $ZrO_2$: monoclinic (no addition) and cubic (10 mol.%), respectively. The precipitate was recovered by filtration, dried at 100 °C and calcined in static air at 600 °C for 5 h.

The prepared supports are hereafter referred as: $ZrO_2$-m – monoclinic and $ZrO_2$-c – cubic, respectively.

### 2.2. Synthesis of $ZrO_2$-supported catalysts

Monometallic catalysts containing 4 wt.% of Pd were prepared by wet impregnation of the previously prepared supports. A solution of a calculated amount of palladium acetate ($Pd(O_2CCH_3)_2$; Sigma–Aldrich) was prepared with chloroform. Then the appropriate amount of support was added to the solution. The impregnated samples were dried at 120 °C overnight and calcined at 400 °C for 1 h in an oxygen atmosphere (60 mL $min^{-1}$), cooled in $N_2$ (60 mL $min^{-1}$) to room temperature, and then reduced in a hydrogen flow (150 mL $min^{-1}$) for 2 h at 400 °C.

Bimetallic CuPd-supported catalysts containing 20 wt.% Cu and 4 wt.% Pd were obtained by sequential impregnation. First, palladium was loaded onto the $ZrO_2$ support, dried and heated under $O_2$ at 400 °C for 2 h. Then copper was impregnated on the $Pd/ZrO_2$ sample using copper nitrate ($Cu(NO_3)_2$; Prolabo) as precursor. These catalysts were calcined at 360 °C in static air for 8.5 h and then reduced in $H_2$ for 2 h at 400 °C. For comparative purposes, a monometallic Cu (20 wt.% Cu) catalyst supported on the previously obtained $ZrO_2$-m carrier was prepared. The same experimental procedure as that used for the impregnation of Cu in the bimetallic $CuPd/ZrO_2$ catalysts was followed.

Monometallic and bimetallic catalysts will be denoted in terms of the metal and the $ZrO_2$ supports used: $M/ZrO_2$-x, where M represents the metal: Pd or CuPd and x stands for the $ZrO_2$ phase, -m or -c, respectively. Thus, the catalyst $CuPd/ZrO_2$-m was prepared from a $ZrO_2$-m support impregnated with Cu and Pd.

### 2.3. Characterization

The physicochemical properties of $ZrO_2$ supports and catalysts were evaluated using a variety of methods. The metal content (Pd and Cu) was determined from ICP-OES. The morphology and qualitative composition was obtained from SEM-EDS. The SEM images were recorded using a high resolution (Schottky) environmental scanning electron microscope with X-ray microanalysis and backscattered electron diffraction pattern analysis.

The structure of $ZrO_2$ supports and catalysts was studied by XRD. The XRD pattern of the selected samples was collected using a PANanlytical X'Pert Pro operating in Bragg-Bretano focusing geometry and using Cu $K\alpha$ radiation at wavelengths Cu $K\alpha_1$ = 1.5406 Å and Cu $K\alpha_2$ = 1.54443 Å. The data was collected at 2θ angles (15–95°), with a step size of 0.017°. The obtained X-ray scans were compared to those of standard database and the phases were assigned comparing the data available in literature. The crystallite size of copper phases present in the investigated solids was based on X-ray diffraction line broadening and calculated by using Scherrer Eq. (2).

$$d = \frac{\beta\lambda}{\beta\cos\theta} \quad (2)$$

where d is the average crystallite size of the Cu specie, B is the Scherrer constant (0.89), λ is the wave length of X-ray beam used, β is the full-with half maximum (FWHM) of diffraction and θ is the Bragg's angle.

Multi point Brunauer-Emmett-Teller (BET) surface area measurements were performed on a Quantachrome Autosorb AS-1 instrument at −196 °C. Prior to the analysis the samples were outgassed in vacuum at 200 °C for 2 h.

XPS analysis was performed using a Kratos AXIS Ultra HSA. Vision and CasaXPS software was used for data acquisition and data analysis, respectively. The analysis was carried out with a monochromatic Al Kα X-ray source (1486.7 eV), operating at 15 kV (90 W), in FAT mode (Fixed Analyzer Transmission), with a pass energy of 40 eV for regions and 80 eV for survey. Data acquisition was performed with a pressure lower than $1.0 \times 10 - 6$ Pa using a charge neutralization system. The binding energies were referenced to the C 1 s line at 285 eV from adventitious carbon. The modelling of the spectra was performed using peak fitting with Gaussian-Lorentzian (30%) peak shape and Shirley type background subtraction.

$H_2$-temperature programmed reduction ($H_2$-TPR) experiments were performed using a ChemBET Pulsar TPR/TPD equipped with a thermal conductivity detector (TCD). In a typical TPR experiment, approximately 50 mg of sample was held by quartz wool and placed in a U-shaped quartz reactor. The sample was heated from 50 °C to 400 °C at a heating rate of 5 °C.$min^{-1}$ under a flow of 10% $H_2$/Ar (50 mL $min^{-1}$). Hydrogen consumption was measured by TCD.

### 2.4. Activity measurements

MSR catalytic tests were performed in a fixed bed reactor (7.25 mm i.d.) at atmospheric pressure with the following experimental conditions: a steam/methanol molar ratio of 1.5 and a contact time of $W_{cat.}/F^0_{CH_3OH} = 83 kg_{cat} \cdot mol^{-1} \cdot s^{-1}$. The reactor was loaded with 400 mg of catalyst (180–350 μm) and diluted with 800 mg of glass beads. The micro-reactor was placed in the electrically heated furnace and the temperature was controlled by placing a temperature controller inside the furnace as well as inside the micro-reactor through a K-type thermocouple inserted into the catalytic bed. Plug flow conditions were ensured keeping catalyst bed length to catalyst size ratio above 50 ($L_{reactor}/d_{particle} \geq 50$) and the reactor diameter to size ratio above 30 ($D_{reactor}/d_{particle} \geq 30$) [13].

Prior to the catalytic test, the catalyst was reduced in-situ, in a $H_2$ stream (70 vol.%) diluted with $N_2$ at 240 °C for 2 h. Then, the catalyst was cooled down to 180 °C in $N_2$ and the reaction mixture was introduced by a HPLC pump into the reactor. Tests were performed between 180 and 260 °C. Hydrogen and carbon dioxide were analyzed in a quadrupole mass spectrometer (Pfeiffer Vacuum OmniStar GSD 320). During the tests the MS was calibrated using a gas mixture of 80% $N_2$, 15% $H_2$ and 5% $CO_2$. The unreacted methanol and water were separated from the product stream in a condenser at ca. 0 °C, placed outside the oven. Trace amount of carbon monoxide were measured using a CO infra-red analyzer (Signal Instruments, 7100 FM, accuracy: ± 0.2 ppm). The methanol conversion ($X_{CH_3OH}$) and CO output molar fraction ($Y_{CO}$) were calculated by applying Eqs. (3) and (4). The selectivity towards $CO_2$ (also referred as MSR selectivity) and CO was calculated by applying Eq. (5), where

$CO_x$ stands for $CO_2$ or CO. The subscripts *in* and *out* indicate the inlet and the outlet concentrations of the reactants or products.

$$X_{MeOH} = \frac{Q_{CO,out} + Q_{CO_2,out}}{Q_{CH_3OH,in}} \quad (3)$$

$$Y_{CO} = \frac{Q_{CO,out}}{Q_{TOT,out}} \quad (4)$$

$$S_{COx} = \frac{Q_{COx,out}}{\sum Q_{COx,out}} \quad (5)$$

## 3. Results and discussion

As observed in Fig. 1, the $ZrO_2$ support structure has little influence on the performance of the monometallic Pd/$ZrO_2$ catalysts; the use of $ZrO_2$-m results in a slight improvement of both activity and selectivity (lower CO production) when compared with $ZrO_2$-c (Fig. 1). Both Pd/$ZrO_2$-m and Pd/$ZrO_2$-c catalysts present comparable XRD patterns that are dominated by the intense lines of the monoclinic (JCPDS 37-1484) and cubic (JCPDS 27-0997) $ZrO_2$ phases (Figs. 2 and 3). This means that the structure of the $ZrO_2$ support was kept after palladium impregnation. Additional peaks at 40.2° and 46.8° in the Pd/$ZrO_2$-c pattern (Fig. 3) denote the appearance of crystalline metallic palladium ($Pd^0$; JCPDS 87-0639). These reflection lines were not observed in the Pd/$ZrO_2$-m pattern, which evidences a higher Pd dispersion on $ZrO_2$-m, despite the lower BET surface area (Table 1) of this carrier.

The impregnation of Pd causes a slight loss of specific surface area on Pd/$ZrO_2$-c (ca. 9%) but does not produce any significant change on Pd/$ZrO_2$-m (Table 1). The formation of larger Pd crystallites on $ZrO_2$-c, as evidenced by XRD, could explain the decrease of surface area in this sample. The smaller Pd particles formed in $ZrO_2$-m, being highly dispersed, do not change the texture of the bare $ZrO_2$-m, maintaining its initial BET surface area. SEM-EDX data are consistent with these findings. On Pd/$ZrO_2$-c, palladium particles tend to segregate forming isolated Pd clusters over the ZrO2-c surface, as it can be observed in Z2 at Fig. 4-B (Pd/Zr atomic ratio of 0.64%). However, the surface of Pd/$ZrO_2$-m consists of Pd and Zr more homogeneously distributed, although some isolated Pd clusters are also found (Fig. 4-A).

The characterization results of Pd/$ZrO_2$ catalysts evidence a higher dispersion along with an even distribution of palladium on the $ZrO_2$-m support, which might account for its slight better performance. Although the observed differences are small, the results of the monometallic catalysts suggest that the $ZrO_2$ structure might influence the performance of supported Pd/$ZrO_2$ catalysts.

To the best of our knowledge, there are only few examples using Pd/$ZrO_2$ catalysts for MSR [4,8]. Values of 80% of selectivity for a reaction temperature of 220 °C [8] and of 200 °C [14] are reported. It is evident from Fig. 1-B, that our Pd/$ZrO_2$ catalysts allowed a CO selectivity reduction of almost 2-fold when compared with previous reports on Pd/$ZrO_2$-MSR catalysts [8,14].

While these are promising results, the selectivity of Pd/$ZrO_2$ catalysts is still far from that of Cu-based catalysts [2,15–17] and Pd-alloys based catalysts, which are recognized by their high selectivity towards MSR reaction [18]. Actually, the literature reports that the selectivity of supported Pd catalysts for MSR can be significantly improved using Pd alloys [2,18,19], being PdZn [19] and PdGa [18] alloys the most common. However, considering that Cu-based materials are the most active and selective catalysts for MSR, the effect of Cu as promoter for Pd/$ZrO_2$ MSR catalysts was studied.

Contrary to what was observed for monometallic catalysts, the $ZrO_2$ structure, monoclinic or cubic, has a pronounced effect on the performance of the bimetallic CuPd/$ZrO_2$ catalysts (Fig. 5). Compared to Pd/$ZrO_2$ samples, the addition of copper has a positive effect on $ZrO_2$-m while it causes the opposite effect on $ZrO_2$-c (Figs. 1–5).

For instance, for $ZrO_2$-m the addition of Cu resulted in a remarkable increase of the conversion, up to 5-times higher when compared to the unpromoted Pd/$ZrO_2$-m sample, which is accompanied by an astounding improvement of the MSR selectivity. CuPd/$ZrO_2$-m is up to 8-times more selective than the unpromoted catalyst in the whole temperature range studied.

Interestingly, the CuPd/$ZrO_2$-m catalyst is also significantly more selective towards MSR than CuPd/$ZrO_2$-c (at 180 °C, MSR selectivity over CuPd/$ZrO_2$-m is up to 2-times higher when compared to its homologous CuPd/$ZrO_2$-c, increasing up to 4-times at 260 °C). This represents a remarkable reduction of the CO concentration (compare Figs. 1B–5B). These are in fact quite good results, particularly if CuPd/$ZrO_2$-m catalyst is considered for the production of hydrogen for PEM fuel cells, where the CO content has to be lowered as much as possible to prevent damage to the Pt electro catalyst. Regarding methanol conversion, CuPd/$ZrO_2$-m catalyst is also much more active than CuPd/$ZrO_2$-c, particularly at very low temperature (180–200 °C, Fig. 5). For instance at 180 °C CuPd/$ZrO_2$-c is not able to convert methanol but CuPd/$ZrO_2$-m shows a conversion of about 20%, which is a huge improvement.

These results show that the addition of copper to the Pd/$ZrO_2$-m catalyst promotes both the catalytic activity and selectivity towards MSR, giving rising to a bimetallic CuPd/$ZrO_2$-m catalyst with enhanced performances compared not only to the unpromoted Pd catalyst but also to the bimetallic $ZrO_2$-c supported one. In view of these remarkable results and considering that Cu catalysts are still by far the most commonly used catalysts for MSR, it seems quite logical to study the catalytic behavior of the monometallic Cu/$ZrO_2$-m system. With this aim, a monometallic Cu/$ZrO_2$-m sample (20 wt.% Cu) prepared following the same experimental procedure described in Section 2.2 was studied in MSR. Fig. 6A compares the activity of both $ZrO_2$-m supported catalysts at different temperatures. As apparent in this figure, the bimetallic CuPd/$ZrO_2$-m sample showed the highest activity in the entire temperature range explored. These results demonstrate that, at least in the conditions of the present study, there is a cooperative effect between Cu and Pd metals, which might account for the enhanced performances of the CuPd/$ZrO_2$-m catalyst.

It is clear that CuPd/$ZrO_2$-m displays excellent performances for MSR, not only in terms of activity but also and even more significant in terms of MSR selectivity. This sample also shows good stability for 80 h on stream (Fig. 6B). Despite comparison with other reported MSR systems is difficult because of the different operating conditions, it is interesting to highlight that our CuPd/$ZrO_2$-m catalyst shows better results than other highly performing Pd-MSR catalysts. A CO selectivity of around 10% is reported for PdZn/ZnO and $Pd_2Ga/Ga_2O_3$ systems at 180–250 °C [18]. The CuPd/$ZrO_2$-m catalyst studied in the present work has a CO selectivity of around 5%. This demonstrates that our CuPd/$ZrO_2$-m catalyst exhibits very good MSR selectivity, which is nearly constant in the considered temperature range (180–260 °C).

The enhancement of MSR selectivity observed after Cu addition to the unpromoted Pd/$ZrO_2$ catalysts, is attributed to the different MSR reaction mechanism for Pd- (and group VIII metals) and Cu-containing catalysts. Over Pd catalysts, the intermediate carbonyl formed after methanol adsorption on the metallic palladium sites adopts preferentially a bidentate conformation, which then decomposes and desorbs as CO [2,14]. Whilst, over Cu-based catalysts the intermediate formed over Cu-sites has a monodentate structure and is simply desorbed as $CO_2$, without decomposition [2]. This makes Cu-based samples very selective towards MSR while Pd and group VIII metals would preferentially catalyse MD producing CO instead of $CO_2$.

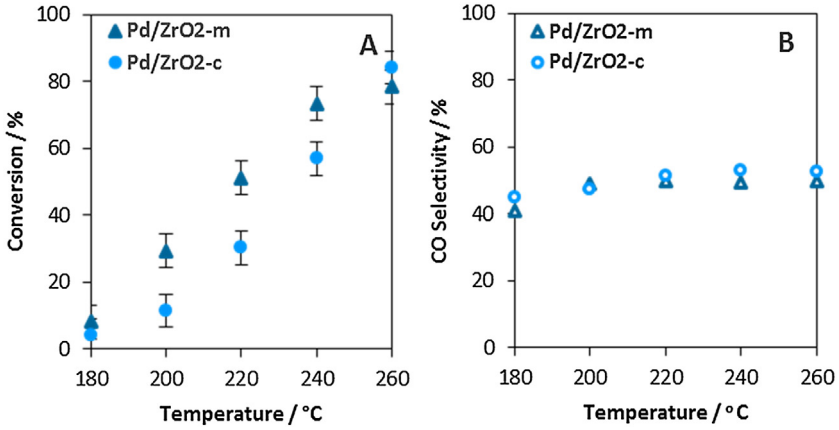


**Fig. 1.** (A) Methanol conversion (%) and (B) CO selectivity (%) as a function of the temperature for the series of $Pd/ZrO_2$ catalysts.

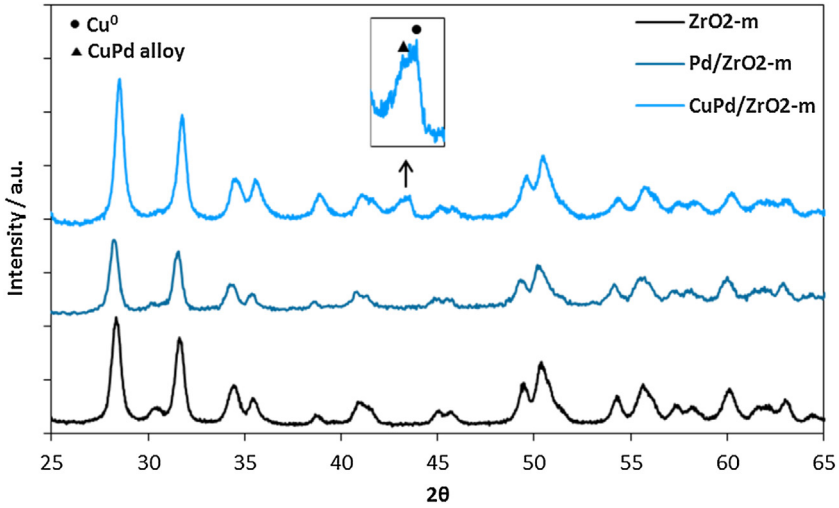


**Fig. 2.** XRD patterns of $ZrO_2$-m carrier and $ZrO_2$-m supported catalysts. CuPd alloy (JCPDS card no. 48-1551).

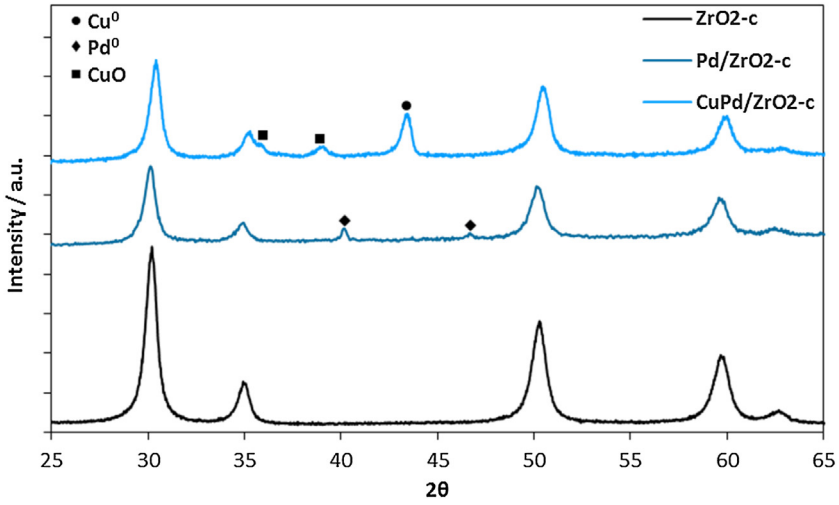


**Fig. 3.** XRD patterns of $ZrO_2$-c carrier and $ZrO_2$-c supported catalysts; $Cu^0$ (JCPDS card no. 85–1326); $Pd^0$ (JCPDS card no. 87-0639). CuO (JCPDS card no. 48-1548).

As already mentioned, the bimetallic catalysts present large differences in CO selectivity (Fig. 5-B). While the CO selectivity does not change with temperature for $CuPd/ZrO_2$-m (Fig. 5-B), it increases linearly with temperature for $CuPd/ZrO_2$-c, reaching a maximum value of 23% at 260 °C, which represents an increase of 80% compared to $CuPd/ZrO_2$-m. This cannot be explained by differences in the catalysts composition since both $CuPd/ZrO_2$ samples have the same nominal composition, as confirmed by ICP. So clearly, the structure of $ZrO_2$ influences the MSR selectivity of the $CuPd/ZrO_2$ catalysts, and the use of a monoclinic

**Table 1**
Physicochemical properties of both supports and catalysts.

| Sample | $S_{BET}$ ($m^2\ g^{-1}$) | Cu surface area ($m^2\ g^{-1}$ Cu) | Max. reduction temperature (°C) | [a]Mean Cu crystallite size (nm) |
|---|---|---|---|---|
| $ZrO_2$-m | 23 | – | – | – |
| Cu/$ZrO_2$-m | – | – | 263 | – |
| Pd/$ZrO_2$-m | 24 | – | 219 | – |
| CuPd/$ZrO_2$-m | 15 | 61.3 | 105 | 19 |
| $ZrO_2$-c | 53 | – | – | – |
| Cu/$ZrO_2$-c | – | – | 236 | – |
| Pd/$ZrO_2$-c | 46 | – | 219 | – |
| CuPd/$ZrO_2$-c | 28 | 15.4 | 90 ($Pd^{2+}$) and 140 ($Cu^{2+}$) | 51 |

[a] Average Cu crystallite size derived from XRD.

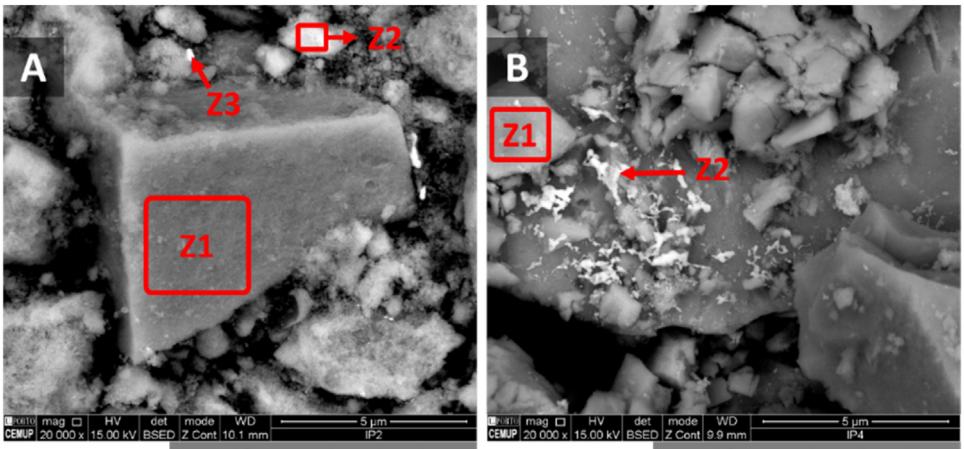


| | Pd/Zr atomic ratio (%) |
|---|---|
| **Z1** | 0.09 |
| **Z2** | 0.10 |
| **Z3** | 0.74 |

| | Pd/Zr atomic ratio (%) |
|---|---|
| **Z1** | 0.04 |
| **Z2** | 0.64 |

**Fig. 4.** SEM images of the (A) Pd/$ZrO_2$-m and (B) Pd/$ZrO_2$-c catalysts, with EDX quantification.

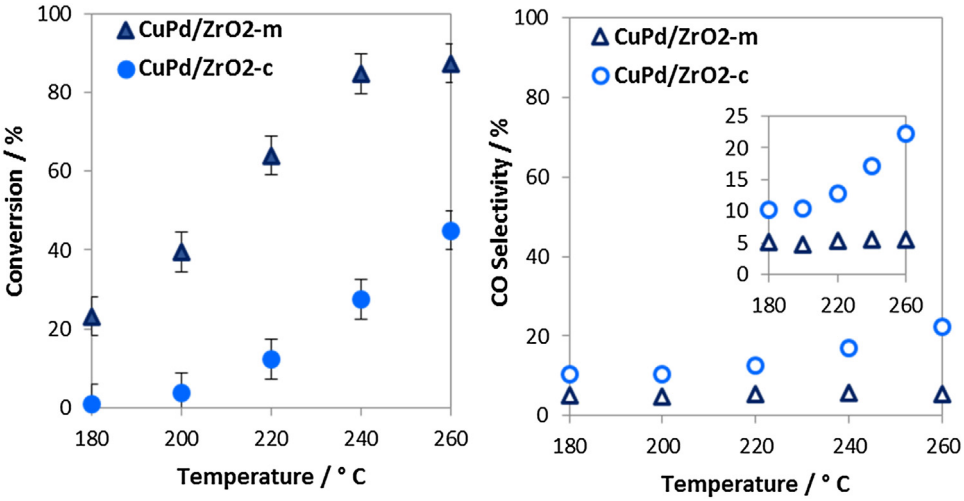


**Fig. 5.** (A) Methanol conversion (%) and (B) CO selectivity (%) as a function of the temperature for the series of CuPd/$ZrO_2$ catalysts.

$ZrO_2$ carrier allows obtaining catalysts with improved MSR selectivity.

In order to shed some light on this, the bimetallic catalysts were thoroughly characterized by $H_2$-TPR, XRD, SEM-EDX, $N_2O$ chemisorption and XPS. For comparative purposes, characterization of the unpromoted Pd/$ZrO_2$ catalysts was performed in some cases.

It is well accepted that the conversion of Cu-containing catalysts for MSR is related to the copper surface area and dispersion. In general the larger the copper surface area the higher the dispersion and so the higher is the conversion. The copper surface area and dispersion for both CuPd/$ZrO_2$ catalysts determined by $N_2O$ chemisorption show considerably lower values for CuPd/$ZrO_2$-c, which could account for its lower performance (61.3 $m^2\ g^{-1}$ Cu for CuPd/$ZrO_2$-m and 15.4 $m^2\ g^{-1}$ Cu for CuPd/$ZrO_2$-c, Table 1).

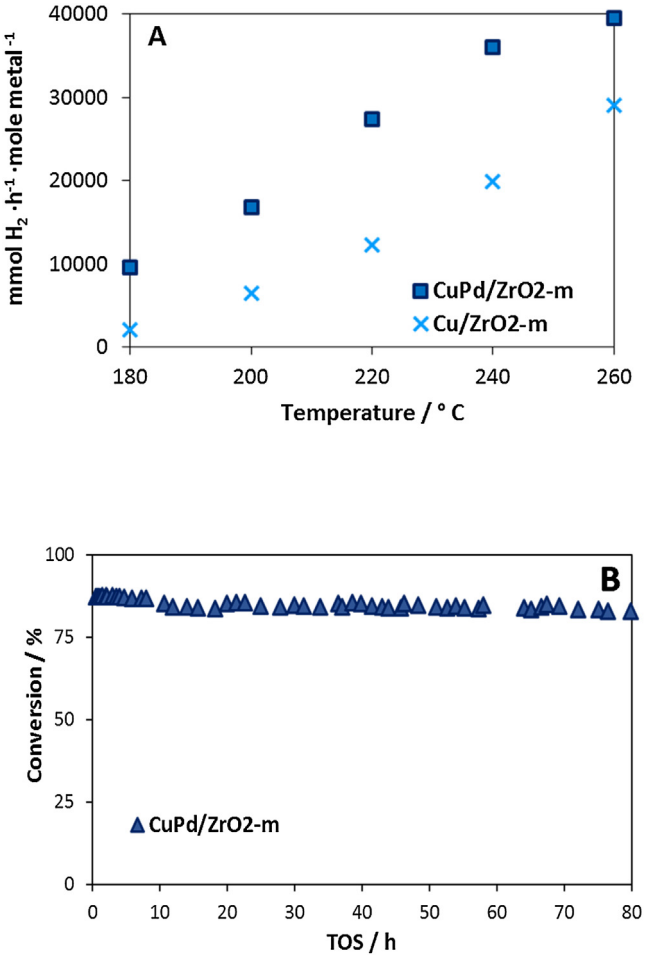


**Fig. 6.** (A) Activity as a function of the temperature for supported $ZrO_2$-m catalysts, Cu/$ZrO_2$-m and CuPd/$ZrO_2$-m; activity was calculated as mmol of hydrogen produced per hour per mole of metal; (B) Evolution of the methanol conversion with time-on-stream (TOS) over CuPd/$ZrO_2$-m, at 240 °C, P = 1 atm, and contact time: $W_{cat.}/F^0_{CH_3OH} = 83 kg_{cat} \cdot mol^{-1} \cdot s^{-1}$.

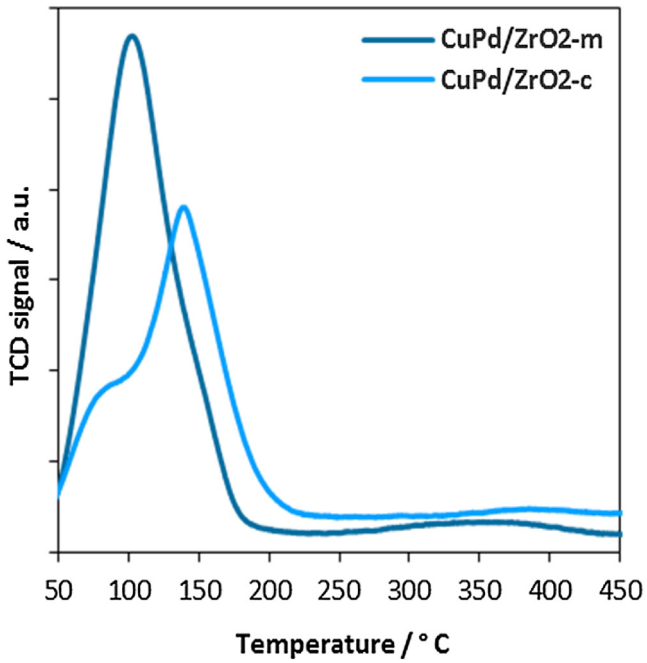


**Fig. 7.** TPR profiles of CuPd/$ZrO_2$-m and CuPd/$ZrO_2$-c catalysts.

The $H_2$-TPR profiles of the monometallic Pd/$ZrO_2$ catalysts (not shown) exhibit negative peaks below 100 °C, ascribed to the presence of palladium hydrides, which are not observed in the TPR curves of the bimetallic catalysts. Palladium is reduced at ca. 220 °C over both $ZrO_2$ supports (Table 1). $H_2$-TPR experiments conducted over Cu supported on the same $ZrO_2$ carriers evidence that copper is reduced below 300 °C on both Cu/$ZrO_2$ catalysts, although the higher area of the TPR peak of Cu/$ZrO_2$-c suggests an ease reducibility. TPR curves for bimetallic CuPd/$ZrO_2$ catalysts are presented in Fig. 7. The TPR profile of CuPd/$ZrO_2$-m exhibits a single peak centered at 105 °C. The TPR curve of CuPd/$ZrO_2$-c shows two peaks, the main peak at 140 °C (81% of the whole peak area) and the smaller one at around 90 °C. It is clear that the addition of copper to the Pd/$ZrO_2$ catalysts promotes reducibility, but it affects in a different way depending on the $ZrO_2$ structure.

The presence of a single sharp peak for CuPd/$ZrO_2$-m suggests the existence of one type of species. Similarly, the two reduction peaks in the TPR profile of CuPd/$ZrO_2$-c suggest the presence of two different species. The results for the monometallic systems show that Pd is reduced at lower temperature than Cu, regardless of the $ZrO_2$ carrier. Based on this, the two peaks in the TPR of CuPd/$ZrO_2$-c were ascribed to the reduction of $Pd^{2+}$ (low temperature peak) and $Cu^{2+}$ species (high temperature peak), which might exist as separate phases, likely PdO and CuO. From the relative intensity of both reduction peaks it was concluded that the fraction of Cu-species is larger, in good agreement with the higher Cu content in the catalysts. Anyway, the reduction temperature of Pd and Cu in the CuPd/$ZrO_2$-c catalyst is significantly lower compared to its monometallic counterparts, Pd/$ZrO_2$-c and Cu/$ZrO_2$-c, which was ascribed to the lower temperature reduction of Pd and Cu clusters present in CuPd/$ZrO_2$-c. On the other hand, CuPd/$ZrO_2$-m sample displays a reduction temperature comprised between that ascribed to the reduction of relatively small Cu crystallites (ca. 140 °C, TPR of CuPd/$ZrO_2$-c) and Pd (ca. 90 °C, TPR of CuPd/$ZrO_2$-c). From this data and considering that CuPd/$ZrO_2$-m shows only one reduction peak, the peak at 105 °C in the TPR of CuPd/$ZrO_2$-m was attributed to the reduction of palladium and copper species in strong interaction.

TPR results seem then to point that Pd and Cu strongly interact when supported on $ZrO_2$-m but they tend to segregate as separate oxides when supported on $ZrO_2$-c. This is in good agreement with XRD findings. The presence of a broad peak at 42.5° in the pattern of CuPd/$ZrO_2$-m, which was ascribed to a CuPd alloy (JCPDS 48-1551) Fig. 3, evidences the existence of a CuPd strong interaction, supporting our previous assumptions. The main lines of $ZrO_2$-m and a broad reflection at 43.5° characteristic of metallic copper (JCPDS 85-1326) are also found in the pattern of CuPd/$ZrO_2$-m. In the case of CuPd/$ZrO_2$-c sample, only intense reflections of metallic copper (JCPDS 85-1326) and $ZrO_2$-c are observed (Fig. 3). The presence of sharper $Cu^0$ lines in CuPd/$ZrO_2$-c suggests higher crystallinity and thus larger crystallites of $Cu^0$ in this sample, in good agreement with its lower dispersion, as proved by $N_2O$ chemisorption.

SEM images of CuPd/$ZrO_2$-c sample shows a heterogeneous surface, where Cu-rich regions coexist with Zr-rich and CuPd-rich spots (Fig. 8), in acordance with TPR findings. Contrarily, the surface of CuPd/$ZrO_2$-m consists of Cu, Pd and Zr homogeneously distributed, suggesting again the existence of Cu and Pd particles highly dispersed and in intimitate contact.

XPS technique was used to obtain information on the chemical state of Pd and Cu and on the surface composition of the CuPd/$ZrO_2$ samples after the reduction step. To study the effect of copper in bimetallic catalysts, in particular, if Pd electronic properties were affected by the presence of Cu, unpromoted Pd/$ZrO_2$ samples were also characterized by XPS. The binding energy (BE)

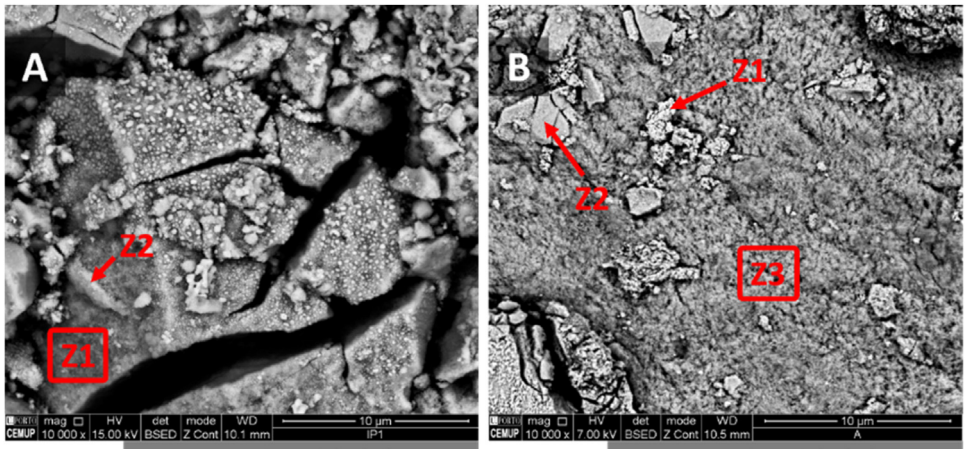


| | Atomic weight (%) | | |
|---|---|---|---|
| | Cu | Pd | Zr |
| Z1 | 8.2 | 1.1 | 22.5 |
| Z2 | 12.7 | 2.1 | 24.4 |

| | Atomic weight (%) | | |
|---|---|---|---|
| | Cu | Pd | Zr |
| Z1 | 61.5 | 38.5 | 0.0 |
| Z2 | 18.8 | 3.1 | 24.4 |
| Z3 | 55.3 | 0.0 | 0.0 |

**Fig. 8.** SEM images of the (A) CuPd/$ZrO_2$-m and (B) CuPd/$ZrO_2$-c catalysts, with EDX quantification.

**Table 2**
Bulk and surface atomic ratios for reduced Pd/$ZrO_2$ and CuPd/$ZrO_2$ samples. $Zr3d_{5/2}$, $Pd3d_{5/2}$, $Cu2p_{3/2}$ Binding Energy (BE) for Pd/$ZrO_2$ and CuPd/$ZrO_2$ catalysts.

| Sample | Cu/Zr | | Pd/Zr | | BE (eV) $Zr3d_{5/2}$ | BE (eV) $Pd3d_{5/2}$ | BE (eV) $Cu2p_{3/2}$ | [c]a' (eV) |
|---|---|---|---|---|---|---|---|---|
| | Bulk[a] | XPS[b] | Bulk[a] | XPS[b] | | | | |
| CuPd/$ZrO_2$-m | 0.83 | 0.84 | 0.10 | 0.08 | 182.1 | 335.7 | 932.6 | 1851.8 |
| Pd/$ZrO_2$-m | 0.83 | – | 0.10 | 0.11 | 182.2 | 335.0 | – | – |
| CuPd/$ZrO_2$-c | 0.83 | 0.98 | 0.10 | 0.06 | 182.1 | 335.1 | 932.6 | 1849.5 |
| Pd/$ZrO_2$-c | 0.83 | – | 0.10 | 0.18 | 182.1 | 335.0 | – | – |

[a] The relative concentrations have been calculated from ICP analysis.
[b] The relative concentrations have been calculated from the XPS data.
[c] The modified Auger parameter for Cu, derived from XPS data.

values of $Pd3d_{5/2}$, $Cu2p_{3/2}$ and $Zr3d_{5/2}$ and the surface composition for the various samples are compiled in Table 2.

For CuPd/$ZrO_2$-c the XPS Cu/Zr ratio is much higher than that of the bulk, which could be attributed to the larger Cu crystallites in this sample, as inferred from XRD. For CuPd/$ZrO_2$-m the XPS Cu/Zr ratio matches the bulk ratio, confirming the higher dispersion of copper in this sample evidenced by other techniques. The higher Pd/Zr XPS ratio of CuPd/$ZrO_2$-m with regard to CuPd/$ZrO_2$-c, suggests a higher dispersion of Pd on the latter sample, in good agreement with TPR and SEM results.

The BE of $Pd3d_{5/2}$ for monometallic Pd/$ZrO_2$ samples has a value of 335.0 eV indicating that Pd should be in the reduced state, as $Pd^0$ [20]. $Pd3d_{5/2}$ BE was 335.7 eV and 335.1 eV for CuPd/$ZrO_2$-m and CuPd/$ZrO_2$-c, respectively. Clearly, the CuPd/$ZrO_2$-m sample shows a significant shift of Pd BE (by 0.7 eV) to a higher value, suggesting the existence of a strong electronic interaction between Pd and Cu, such as would be found in PdCu alloy formation. This positive shift can be attributed to the charge transfer between Pd and Cu elements as a consequence of the strong interaction between these metals, i.e. alloy formation, as already described in previous studies [21]. These results confirm the existence of a strong interaction between Cu and Pd in CuPd/$ZrO_2$-m evidenced by other techniques. XPS results demonstrate that the strong Cu-Pd interaction modifies the electronic properties of Pd in CuPd/$ZrO_2$-m, which could account for the improvement of MSR selectivity of this catalyst. Similarly, the BE value of 335.1 eV observed for $Pd3d_{5/2}$ in CuPd/$ZrO_2$-c, typical of $Pd^0$ species [20], with the absence of any significant shift, seems to confirm that Pd and Cu are not strongly interacting in this sample, in good agreement with previous data. According to these results, the electronic properties of Pd and Cu are not significantly modified, and they keep their individual properties. This could explain the trend in MSR selectivity shown by CuPd/$ZrO_2$-c. It presents a higher MSR selectivity than Pd/$ZrO_2$-c due to the presence of Cu, which selectively catalyze MSR reaction decreasing CO production, but it is greatly less selective towards MSR than CuPd/$ZrO_2$-m due to the lack of Cu-Pd strong interaction.

The peak-fit of the Cu $2p_{3/2}$ in CuPd/$ZrO_2$ samples gives a BE of 932.6 eV. It is difficult to differentiate between $Cu^0$ and $Cu^+$ species based on their $Cu2p_{3/2}$ BE, which are nearly identical (~932.2 eV for $Cu^+$ and ~932.4 eV for $Cu^0$). As a result, the kinetic energies of the Cu (LMM) Auger peaks are commonly used to distinguish between both types of copper species. The Auger parameter of CuPd/$ZrO_2$-m sample is 1851.8 eV, indicating that $Cu^0$ is the predominant copper species on the surface of this sample. The Auger parameter of CuPd/$ZrO_2$-c is 1849.5 eV ascribed to $Cu^+$. The characterization results suggest that Cu and Pd are strongly interacting, probably as a CuPd alloy, when supported on $ZrO_2$-m, resulting in a catalyst made up of highly dispersed CuPd clusters with different electronic properties respect to those of each metal on its own. The particular "electronic structure" of these CuPd clusters may result in a different interaction with the reactants, leading to different intermediate species and thus, different MSR reaction mechanism. This would be a similar case to that reported for PdZn and PdGa alloys, where the formation of a specific Pd-alloy promotes the conversion and selectivity towards MRS. The conversion enhancement is attributed to the presence of small Pd-alloy particles that led to better dispersion.

In the present case, a higher dispersion of metals on $ZrO_2$-m was also evidenced by SEM, XPS and XRD, which might account for the better activity of the CuPd/$ZrO_2$-m. The new CuPd/$ZrO_2$-m catalyst has activity and selectivity similar to those based on copper, with the advantage of having higher thermal stability, which is characteristic of Pd catalysts. Thus, it can be stated that this new catalyst overcomes the limitation of the traditional Cu catalysts without compromising its selectivity.

## 4. Conclusions

CuPd/$ZrO_2$-m catalysts with greatly improved MSR performance have been developed. A straightforward approach consisting in Cu addition as promoter and $ZrO_2$-m as support was used. Compared to the unpromoted Pd/$ZrO_2$-m catalyst the addition of Cu leads to an astounding improvement of MSR selectivity by 87%. Concerning CuPd/$ZrO_2$ catalysts, the use of the $ZrO_2$-m support allowed a remarkable enhancement of both MSR activity and selectivity, particularly at low temperature (<220 °C). At 180 °C CuPd/$ZrO_2$-m is up to 13-times more active and 2-times more selective towards MSR than CuPd/$ZrO_2$-c. This superior performance was attributed to a strong interaction between Pd and Cu and an enhanced dispersion of the metal phase when $ZrO_2$ with monoclinic structure was used as support. These are indeed outstanding results that have not been previously reported to the best of our knowledge.

## Acknowledgements

The research leading to these results has received funding from the European Union's Seventh Framework Programme (FP/2007-2013) for the Fuel Cells and Hydrogen Joint Technology Initiative under grant agreement no. [303476]. Part of this work was financially supported by: Project POCI-01-0145-FEDER-006939 (Laboratory for Process Engineering, Environment, Biotechnology and Energy – LEPABE funded by FEDER funds through COMPETE2020 – Programa Operacional Competitividade e Internacionalização (POCI). Dra C. Mateos-Pedrero is grateful to the Portuguese Foundation for Science and Technology (FCT) for her Post-Doctoral Grant (Ref.: SFRH/BPD/97114/2013). Mr. A. Gutiérrez from FEUP is acknowledged for performing MSR activity tests. CEMUP and SEMAT are also thanked.

## References

[1] S.D. Jones, H.E. Hagelin-Weaver, Steam reforming of methanol over CeO2- and ZrO2-promoted Cu-ZnO catalysts supported on nanoparticle Al2O3, Appl. Catal. B Environ. 90 (2009) 195–204, http://dx.doi.org/10.1016/j.apcatb.2009.03.013.
[2] S. Sá, H. Silva, L. Brandão, J.M. Sousa, A. Mendes, Catalysts for methanol steam reforming—a review, Appl. Catal. B Environ. 99 (2010) 43–57, http://dx.doi.org/10.1016/j.apcatb.2010.06.015.
[3] G.A. Olah, A. Goeppert, G.K.S. Prakash, Beyond Oil and Gas: The Methanol Economy, Wiley-VCH Verlag GmbH & Co KGaA, Weinheim, Germany, 2009, http://www.scopus.com/inward/record.url?eid=2-s2.0-84889612985&partnerID=tZOtx3y1 (accessed 30.03.15).
[4] R. Pérez-Hernández, a. D. Avendaño, E. Rubio, V. Rodríguez-Lugo, Hydrogen production by methanol steam reforming over Pd/ZrO2–TiO2 catalysts, Top. Catal. 54 (2011) 572–578, http://dx.doi.org/10.1007/s11244-011-9622-0.
[5] K. Eblagon, P. Concepción, Ultraselective low temperature steam reforming of methanol over PdZn/ZnO catalysts—influence of induced support defects on catalytic performance, Appl. Catal. B Environ. 154–155 (2014) 316–328, http://dx.doi.org/10.1016/j.apcatb.2014.02.032.
[6] A.M. Karim, T. Conant, A.K. Datye, Controlling ZnO morphology for improved methanol steam reforming reactivity, Phys. Chem. Chem. Phys. 10 (2008) 5584–5590, http://dx.doi.org/10.1039/b800009c.
[7] Y.-H. Chin, Y. Wang, R.a. Dagle, X. Shari Li, Methanol steam reforming over Pd/ZnO: catalyst preparation and pretreatment studies, Fuel Process. Technol. 83 (2003) 193–201, http://dx.doi.org/10.1016/S0378-3820(03)00067-5.
[8] N. Iwasa, N. Takezawa, New supported Pd and Pt alloy catalysts for steam reforming and dehydrogenation of methanol, Top. Catal. 22 (2003) 215–224, http://dx.doi.org/10.1023/A:1023571819211.
[9] C. Chang, J. Wang, C. Chang, Effect of ZrO2 on steam reforming of methanol over CuO/ZnO/ZrO2/Al2O3 catalysts, Chem. Eng. J. 192 (2012) 350–356, http://dx.doi.org/10.1016/j.cej.2012.03.063.
[10] I. Ritzkopf, S. Vukojević, C. Weidenthaler, J.-D. Grunwaldt, F. Schüth, Decreased CO production in methanol steam reforming over Cu/ZrO2 catalysts prepared by the microemulsion technique, Appl. Catal. A Gen. 302 (2006) 215–223, http://dx.doi.org/10.1016/j.apcata.2006.01.014.
[11] T. Witoon, J. Chalorngtham, P. Dumrongbunditkul, M. Chareonpanich, J. Limtrakul, CO2 hydrogenation to methanol over Cu/ZrO2 catalysts: effects of zirconia phases, Chem. Eng. J. 293 (2016) 327–336, http://dx.doi.org/10.1016/j.cej.2016.02.069.
[12] X. Bokhimi, A. Morales, A. Garcíía-Ruiz, T.D. Xiao, H. Chen, P.R. Strutt, Transformation of yttrium-Doped hydrated zirconium into tetragonal and cubic nanocrystalline zirconia, J. Solid State Chem. 142 (1999) 409–418, http://dx.doi.org/10.1006/jssc.1998.8056.
[13] G.F. Froment, K.B. Bischoff, Chemical Reactor Analysis and Design, 2nd ed., Wiley, New York, 1990.
[14] N. Iwasa, S. Kudo, H. Takahashi, S. Masuda, N. Takezawa, Highly selective supported Pd catalysts for steam reforming of methanol, Catal. Lett. 19 (1993) 211–216, http://dx.doi.org/10.1007/BF00771756.
[15] D. Hammoud, C. Gennequin, A. Aboukaïs, E.A. Aad, Steam reforming of methanol over x% Cu/Zn–Al 400 500 based catalysts for production of hydrogen: preparation by adopting memory effect of hydrotalcite and behavior evaluation, Int. J. Hydrogen Energy 40 (2015) 1283–1297, http://www.sciencedirect.com/science/article/pii/S0360319914026391 (accessed 28.12.15).
[16] E. Linga Reddy, H.C. Lee, D.H. Kim, Steam reforming of methanol over structured catalysts prepared by electroless deposition of Cu and Zn on anodically oxidized alumina, Int. J. Hydrogen Energy. 40 (2015) 2509–2517, http://dx.doi.org/10.1016/j.ijhydene.2014.12.094.
[17] E. Linga Reddy, J. Karuppiah, H.C. Lee, D.H. Kim, Steam reforming of methanol over copper loaded anodized aluminum oxide (AAO) prepared through electrodeposition, J. Power Sources 268 (2014) 88–95, http://www.sciencedirect.com/science/article/pii/S0378775314007745 (accessed 12.02.16).
[18] K. Föttinger, The effect of CO on intermetallic PdZn/ZnO and Pd2Ga/Ga2O3 methanol steam reforming catalysts: a comparative study, Catal. Today 208 (2013) 106–112, http://dx.doi.org/10.1016/j.cattod.2012.12.004.
[19] N. Iwasa, S. Masuda, N. Ogawa, N. Takezawa, Steam reforming of methanol over Pd/ZnO: effect of the formation of PdZn alloys upon the reaction, Appl. Catal. A Gen. 125 (1995) 145–157, http://dx.doi.org/10.1016/0926-860X(95)00004-6.
[20] R. Van Grieken, A. Markowicz, Handbook of X-Ray Spectrometry, 2001.
[21] C. Hu, X. Zhai, Y. Zhao, K. Bian, J. Zhang, L. Qu, H. Zhang, H. Luo, Small-sized PdCu nanocapsules on 3D graphene for high-performance ethanol oxidation, Nanoscale 6 (2014) 2768–2775, http://dx.doi.org/10.1039/C3NR05722D.